

A dark yellow fluorescent protein (YFP)-based Resonance Energy-Accepting Chromoprotein (REACH) for Förster resonance energy transfer with GFP

Sundar Ganesan^{*†}, Simon M. Ameer-beg[‡], Tony T. C. Ng[§], Borivoj Vojnovic[‡], and Fred S. Wouters^{*†¶}

^{*}Cell Biophysics Group, European Neuroscience Institute–Göttingen, Waldweg 33, 37073 Göttingen, Germany; [†]Advanced Technology Development Group, Gray Cancer Institute, Mount Vernon Hospital, Northwood, Middlesex HA6 2JR, United Kingdom; and [§]King's College London, Randall Centre, New Hunt's House, Guy's Medical School Campus, London SE1 1UL, United Kingdom

Edited by Erwin Neher, Max Planck Institute for Biophysical Chemistry, Göttingen, Germany, and approved January 20, 2006 (received for review November 15, 2005)

Förster resonance energy transfer (FRET) microscopy is a powerful technique that enables the visualization of signaling intermediates, protein interactions, and protein conformational and biochemical status. With the availability of an ever-increasing collection of fluorescent proteins, pairs of spectrally different variants have been used for the study of FRET in living cells. However, suitable spectral overlap, necessary for efficient FRET, is limited by the requirement for proper emission separation. Currently used FRET pairs represent compromises between these opposing spectral demands that reduce the maximally attainable FRET sensitivity. We present a previously undescribed FRET acceptor, a nonfluorescent yellow fluorescent protein (YFP) mutant called REACH (for Resonance Energy-Accepting Chromoprotein). REACH allows the use of the photophysically superior FRET donor EGFP, with which it exhibits optimal spectral overlap, which obviates the need for narrow spectral filtering and allows additional fluorescent labels to be used within the same cell. The latter allows the generation of sophisticated bioassays for complex biological questions. We show that this dark acceptor is ideally suited for donor fluorescence lifetime imaging microscopy (FLIM) and confirm these measurements with an independent intensity-based donor fluorescence quenching resonance energy transfer (FqRET) assay. REACH also can be used in donor photobleaching kinetics-based FRET studies. By detecting FRET between a GFP-tagged ubiquitination substrate and REACH-labeled ubiquitin, we imaged the active ubiquitination machinery inside cells. This assay therefore can be used to study proteins whose function is regulated by ubiquitination.

biosensor | fluorescence lifetime imaging microscopy | ubiquitin | proteasome

Fluorescent protein-based Förster resonance energy transfer (FRET) (1) assays allow the detection and quantification of a variety of cellular biochemical events, e.g., GTPase activity status, protein phosphorylation, degradation, conformational changes, and interactions (2, 3). Spectral contamination, i.e., donor emission bleed-through and direct acceptor excitation, complicates the measurement of FRET between fluorescent protein conjugates and reduces the dynamic range and sensitivity even when both fluorophores are included in the same reporter construct. The ideal FRET couple should possess a large spectral overlap between donor emission and acceptor absorption but separated emission spectra to allow their selective imaging. Because of the relatively broad emission spectra and small Stokes shift, fluorescent proteins generally fail to fulfill these criteria.

The most used FRET pair is a cyan fluorescent protein (CFP) donor and a yellow fluorescent protein (YFP) acceptor (3, 4). CFP furthermore suffers from a reduced fluorescence yield when compared with most members of the fluorescent protein family (5). Moreover, its excitation at low wavelengths causes substantial autofluorescence in cells and is not compatible with commonly used laser lines. Finally, CFP fluorescence exhibits double-exponential

decay that limits its use for fluorescence lifetime imaging microscopy (FLIM). The recently described Cerulean CFP mutant aimed at improving some of these drawbacks (6). It possesses a 2-fold increase in extinction coefficient and was reported to exhibit less complex decay kinetics. Another recent improvement was the discovery of a new cyan-emitting protein from stony coral, MiCy, with greatly improved fluorescence quantum yield (0.9; enhanced CFP = 0.4) and apparently single lifetime (7). However, MiCy forms a tight dimer, which limits its use as fusion partner for proteins. An orange-emitting mKO variant was monomerized to yield a high-molar-extinction coefficient acceptor for MiCy.

GFP is a spectrally superior donor to CFP in many respects. Its absorption/emission characteristics produce higher fluorescence yields in a spectral window that generates less autofluorescence. Furthermore, GFP emission decays monoexponentially, allowing sensitive and quantitative detection of FRET by lifetime imaging (8–12). These characteristics have prompted the search for fluorescent protein acceptors with suitable absorption wavelengths for a GFP donor. An example is the use of red fluorescent proteins (13). However, some red fluorescent proteins have broad absorption spectra that can increase their direct excitation overlap, limiting their use in FRET experiments that rely on sensitized emission. Moreover, they are generally less photostable and bright. A recent study describes the generation of a number of monomeric red-shifted mutants by somatic hypermutation (14, 15). Some of these proteins might prove to possess the proper photophysical properties to allow their use as FRET acceptor with GFP.

YFP has also been used as FRET acceptor for a GFP donor (16). This pair exhibits an exceptionally large spectral overlap. Here, the lifetime of YFP increases in a GFP–YFP couple that undergoes FRET. However, unless spectral unmixing approaches are used (17), their spectral inseparability can obscure this effect by the presence of unpaired GFP and YFP. This method is therefore most suited for intramolecular FRET biosensors that incorporate both GFP and YFP. The use of the “classical” *Aequoria victoria* fluorescent proteins as fusion probes has the advantage of more than a decade of experience in live cell microscopy in a variety of cells, tissues, and animals. We decided to modify enhanced YFP (EYFP) to obtain a genetically encoded optimized acceptor for a GFP donor in FRET microscopy.

Conflict of interest statement: No conflicts declared.

This paper was submitted directly (Track II) to the PNAS office.

Abbreviations: FLIM, fluorescence lifetime imaging microscopy; FRET, Förster resonance energy transfer; FqRET, fluorescence quenching resonance energy transfer; REACH, Resonance Energy-Accepting Chromoprotein; CFP, cyan fluorescent protein; YFP, yellow fluorescent protein; EYFP, enhanced YFP; TEV, tobacco etch virus; HA, hemagglutinin.

[†]Present address: Laboratory of Developmental Neurobiology, National Institute of Child Health and Human Development, Porter Neuroscience Research Center, 35 Convent Drive, MSC 3714, Bethesda, MD 20892.

[¶]To whom correspondence should be addressed. E-mail: fred.wouters@gwdg.de.

© 2006 by The National Academy of Sciences of the USA

Table 1. Spectral characteristics of REACH mutations

Mutation	Name	Excit. max., nm	Excit. half-width, nm	Emission max., nm	Rel. fluor.	Rel. absorp.	R_0 ,* nm
—	EYFP	514	50	533	1.00	1.00	5.6
H148V	—	515	46	532	0.18	0.85	5.4
Y145W	REACH1	495	62	530	0.02	1.06	5.6
H148V+Y145W	REACH2	510	65	538	0.03	1.20	5.9

Excit., excitation; max., maximum; Rel. fluor., relative fluorescence; Rel. absorp., relative absorption.
*As acceptor for GFP.

FRET pairs from the published (5) quantum yield of EGFP (0.6) and molar extinction coefficient of EYFP ($83.4 \text{ mM}^{-1}\text{cm}^{-1}$ at 514 nm) and the absorption and emission spectra of REACH mutants. The orientation factor κ^2 and refractive index were assumed to be 2/3 and 1.33, respectively (see ref. 19 for an overview of the estimation procedure). The R_0 distance of GFP with REACH1 (5.6 nm) and REACH2 (5.9 nm) is increased in comparison to CFP-YFP (4.9 nm), and the R_0 distance of REACH2 exceeds that of GFP-YFP (5.6) (19).

We tested our GFP-REACH FRET pair on a recombinant intramolecular FRET construct consisting of GFP and REACH1, fused by a recognition peptide for the tobacco etch virus (TEV) protease. FRET is lost upon cleavage of this linker sequence. The GFP emission increased 2.2-fold upon incubation with TEV protease, indicative of the presence of 55% FRET in the intact construct (Fig. 1D). This increase was not present upon TEV treatment of a construct lacking the TEV site, but can still be achieved by cleavage of the susceptible flexible linker sequence with the nonspecific proteinase K (data not shown). Importantly, the emission of the TEV construct was increased 2-fold over the entire emission spectrum (see the ratio of emission spectra in Fig. 1D *Inset*), showing that the emission originates exclusively from the GFP donor. Similar results were obtained with a TEV-fusion construct of GFP and REACH2 (data not shown).

A REACH-Based Single-Cell FRET Sensor for Protein Ubiquitination. We designed a FRET assay for the activity of the protein ubiquitination machinery that relies on the interaction between GFP- and REACH-labeled proteins inside cells. For this assay, the GFP donor was fused to the efficient PEST (enriched in proline, glutamic acid, serine, and threonine) ubiquitination substrate (GFP-PEST) (20) and was coexpressed with REACH2-labeled ubiquitin. FRET occurs when REACH-ubiquitin molecules are covalently attached to GFP-PEST. This polyubiquitination modification then targets the GFP-PEST to proteasomes for degradation.

Western blotting of cells expressing REACH2-ubiquitin (≈ 35 kDa) show high-molecular-mass adducts with anti-ubiquitin (Fig. 2E) and anti-GFP antibodies (Abs) (Fig. 2F), indicating that REACH-ubiquitin is accepted by the ubiquitination machinery. The band at ≈ 8 kDa in Fig. 2E represents endogenous ubiquitin, and the band at ≈ 27 kDa represents deubiquitinated REACH chromoprotein (≈ 27 kDa) that escaped proteasomal degradation (Fig. 2F). The GFP-PEST is distributed throughout the cell cytoplasm and, because of its small size, passively enters the nucleus. In addition, small punctate clusters can be observed in the perinuclear region (Fig. 2A). The colocalization of anti-ubiquitin immunoreactivity (Fig. 2B and C) in these clusters establishes these structures as likely proteasomes. Note the comparable distribution of ubiquitin immunoreactivity in untransfected neighboring cells (Fig. 2B), showing that the distribution of proteasomes in cells expressing GFP-PEST is not disturbed. FLIM shows punctate structures with clearly reduced fluorescence lifetimes in the cytoplasm (Fig. 2D), indicating the occurrence of FRET and thus the REACH2-ubiquitination of GFP-PEST. Fluorescence emission was never detected by two-photon microscopy of cells expressing only the

REACH-ubiquitin or nonfused REACH mutants under the imaging conditions used.

One major advantage of REACH is that FLIM (and other donor-based FRET methods) can be performed on photons from the entire spectral range of the donor emission. Therefore, we compared the FLIM analysis of FRET in two spectral emission windows. Fig. 3 shows the fluorescence lifetime distribution of GFP-PEST:REACH2-ubiquitin adducts using a GFP narrow bandpass emission filter (D-F), and the same measurement where the emission filter was omitted (Fig. 3 L-N). Reduced lifetimes can be seen in perinuclear structures (Fig. 3 A, D, I, and L) that are similar to the ubiquitin-containing proteasomes in Fig. 2. In fact, with the location of these proteasomes known from their reduced lifetime, it is possible to recognize these structures also in the GFP fluorescence intensity images (Fig. 3 A and I), even in the background of homogeneous cytoplasmic GFP-PEST. Furthermore, a slight reduction of the fluorescence lifetime, i.e., ubiquitination, can be observed in the cytoplasm. In contrast, omission of coexpressed REACH-ubiquitin causes GFP-PEST emission to exhibit typical non-FRET GFP lifetimes, demonstrating that proteasomal pro-

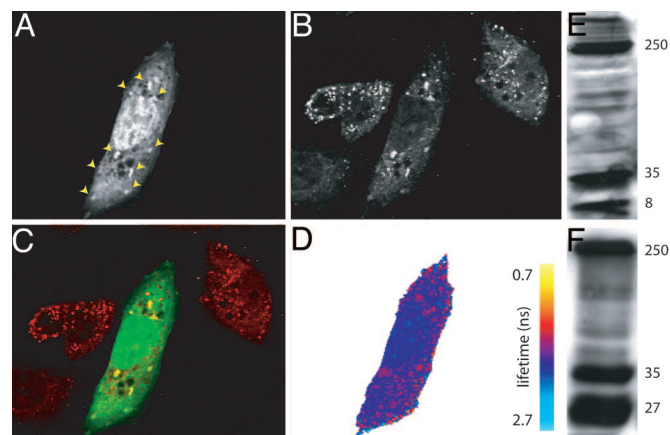


Fig. 2. REACH-ubiquitination of the GFP-PEST substrate in cells. (A) Fluorescence emission distribution of GFP-PEST shows a homogeneous distribution in the cytoplasm in addition to a passive enrichment in the nucleus and higher-intensity structures throughout the cytoplasm (arrowheads). (B) Immunofluorescence staining with anti-ubiquitin Abs identifies the high-intensity GFP structures in A as ubiquitin-rich particles, most likely proteasomes. Shown are cells coexpressing GFP-PEST and REACH2-ubiquitin; four surrounding cells do not express the GFP-PEST. (C) Overlay of GFP-PEST (green channel) and REACH2-ubiquitin (red channel) indicates colocalization (yellow signals) in proteasomal structures. (D) FLIM image of the same cell using two-photon time-correlated single-photon counting imaging shows the presence of low-lifetime signals in cytoplasmic structures, indicative of FRET between GFP-PEST and conjugated REACH-ubiquitin. (E) Western blot of cells expressing GFP-PEST and REACH-ubiquitin with anti-ubiquitin Ab showing free ubiquitin (≈ 8 kDa), REACH-ubiquitin (≈ 35 kDa), and high-molecular-mass adducts (ladder with prominent enrichment at ≈ 250 kDa and higher). (F) Western blot of cells expressing GFP-PEST and REACH-ubiquitin with anti-GFP Ab showing free REACH (≈ 27 kDa), REACH-ubiquitin (≈ 35 kDa), and high-molecular-mass adducts (ladder with prominent enrichment at ≈ 250 kDa).

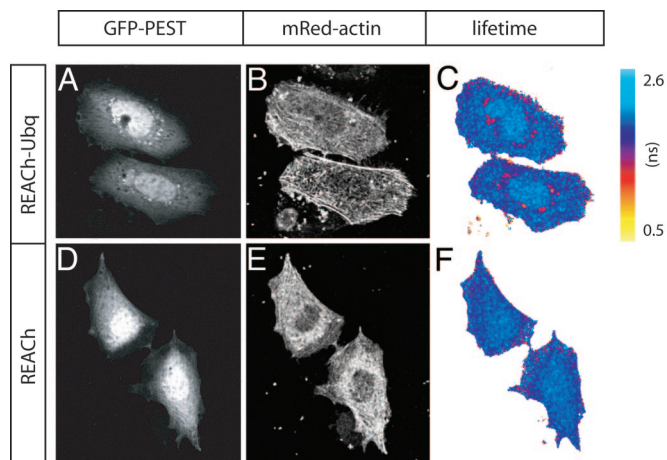


Fig. 4. Simultaneous detection of GFP-PEST ubiquitination and mRed-actin localization. (A and D) Fluorescence emission distribution of GFP-PEST in CHO cells coexpressing REACH2-ubiquitin (A) or control unfused REACH2 (D). (B and E) coexpressed mRed-actin in the same cells expressing REACH2-ubiquitin (B) or unfused REACH2 (E). (C and F) Corresponding GFP lifetime maps for cells expressing the REACH2-ubiquitin (C) or the unfused REACH2 (F).

actions in cells. This FRET pair was used in a protein ubiquitination assay in single cells, both by FLIM and a modified fluorescence quenching resonance energy transfer (FqRET) (21) method that makes use of a dual-dye ubiquitination substrate. The ubiquitination assay reports on the local activity of the ubiquitination machinery but can be used to detect the ubiquitination of other GFP-fusion proteins and can be used to identify new ubiquitination substrates.

Most of the advantages of the use of REACH arise from its absence of fluorescence, which frees the spectral window that a fluorescent acceptor would occupy. Although REACH is not visible in cells, the meaningful readout is the interaction between the donor and acceptor. This finding is inferred from the occurrence of FRET as judged by the altered donor fluorescence properties. In fact, in many FRET assays, the acceptor is commonly present in large excess to saturate donor binding. For most questions, as for our ubiquitination assay, the localization of noninteracting acceptor-labeled proteins does not carry much information. When required, the acceptor can be visualized using Abs against the acceptor-labeled protein, similar to our doubly labeled proteins in the FqRET assay. Alternatively, the acceptor could be additionally tagged with a spectrally separated fluorescent protein. Of course, the need for an additional fluorophore comes at the cost of a decrease in spectral availability.

Our experiments demonstrate the applicability and the advantages of the use of dark chromoproteins as FRET acceptor for GFP. This FRET pair GFP-REACH is superior to the currently favored CFP-YFP combination because of its larger overlap between donor emission and acceptor absorption spectra and enables the use of fluorophores that are not separable otherwise.

The improved detection of FRET is obvious from the R_0 distances of the REACH-GFP pair (5.6 and 5.9 nm), which exceed that of the currently favored CFP-YFP couple (4.9 nm) (22). Assuming a practical FRET detection limit of 5%, up to 9.7-nm separation can be measured compared with 8 nm for CFP-YFP. Moreover, at 8 nm, the FRET efficiency is raised from 5% to 14%, at 7 nm from 10% to 25%, and at 6.2 nm from 20% to 43%, giving rise to a larger dynamic range and higher signal-to-noise level of the determinations.

Because our dark REACH mutants retain their absorptive properties, they present ideal acceptors for FRET; their main advantage in donor-based FRET measurements is that every photon collected

in the donor emission spectral range contributes to the measurement. This property obviates the need for narrow spectral filtering, thereby increasing the signal-to-noise ratio. In our FqRET assay, the Cy5 reference fluorophore effectively also allows the collection of the entire emission band of GFP. Because an acceptor molecule in the excited state cannot accept energy from a donor, the lifetime of the acceptor limits the rate of FRET (23). The extremely short excited-state lifetime of the dark REACH acceptor prevents this effect that might occur at high excitation probabilities, like in laser-scanning microscopy. Furthermore, its extremely short fluorescence lifetime reduces acceptor photobleaching through FRET. High FRET rates and an unfavorable photostability balance between the donor and acceptor can lead to serious degradation of the measured FRET efficiency.

Because the use of a dark acceptor liberates a large part of the optical spectrum, additional fluorescently marked cellular components can be observed. The possibility to correlate FRET events with the behavior of another fluorescent component allows the generation of sophisticated multiplexed bioassays to probe causal connections in the cellular biochemical network. We have shown the feasibility of such extension by the simultaneous detection of mRFP-actin localization and GFP-PEST ubiquitination. More spectrally isolated fluorophores will likely become available from alternative sources for novel fluorescent proteins with improved spectral properties (14, 24–26).

Furthermore, our approach can increase the sensitivity of currently popular donor-acceptor chimeric FRET sensors and play a part in improving the sensitivity, design, and flexibility of FRET assays.

Materials and Methods

Plasmid Construction and Recombinant Protein Purification. pEYFP (Clontech) was subcloned into pRSET-B (Invitrogen) by using NcoI and NotI restriction sites. Sequential site-directed mutagenesis of EYFP was performed with the Quikchange XL kit (Stratagene). The FRET construct for the *in vitro* TEV protease assay comprised a GFP-REACH1, or REACH2 tandem fusion protein, linked by a (GGDYDIPTTENLYFQGG) spacer peptide. The linker contained a TEV recognition site (underlined) and a flanking spacer arm to increase its accessibility to the TEV protease. Additional glycine residues for greater flexibility flanked the spacer peptide. Recombinant TEV protease was from Invitrogen.

Recombinant proteins were purified by immobilized metal affinity chromatography using the 6xHis tag included in the pRSET vector. Constructs were transformed into the BL21DE3 bacterial strain (Stratagene), and liquid cultures were induced with 0.4 mM isopropyl β -D-thiogalactoside at 0.6 OD. Cultures were grown at 25° for 6 h and lysed with Bug-Buster reagent (Novagen). Proteins were purified by using the TALON cobalt affinity resin (Clontech), eluted with 300 mM imidazole and dialyzed against 20 mM Tris-HCl (pH 8.0; TEV construct) or PBS (REACH mutants).

The ubiquitin-REACH fusion constructs were produced by using primer extension PCR amplification of the ubiquitin gene (kind gift of P. van Bergen en Henegouwen, Utrecht University, Utrecht, The Netherlands) introducing flanking BsrGI and NotI sites. The PCR fragment was digested and subcloned into the EYFP-pRSET-B expression vector by using these sites. Next, the EYFP-ubiquitin fusion construct was digested from the resulting vector by using BamHI and NotI restriction enzymes. The resulting fragment was subcloned into similarly digested pEYFP-N1 to replace the original EYFP coding sequence.

Primer extension PCR was used to introduce a HA epitope tag (YPYDVPDYA) at the pd2EGFP C terminus. The pd2EGFP-N1 vector was digested with NotI, treated with Klenow polymerase to produce blunt ends, and was subsequently digested with BamHI. The PCR fragment bearing the HA tag was ligated into the digested pd2EGFP-N1 vector as a BamHI-blunt fragment.

Fluorimetry. Excitation and emission spectra of recombinant REACH1, REACH2, H148V YFP mutant, and EYFP were acquired by using a PTI QM1 Quantamaster T-configuration fluorimeter (Photon Technology International, Monmouth Junction, NJ). Excitation and emission wavelengths were set as described in the figure legends with a slit-width of 1 nm.

Fluorescence Lifetime Microscopy. The fluorescence decays were resolved by time-correlated single-photon counting (TCSPC) using an SPC830 acquisition board (Becker & Hickl, Berlin). Two-photon excitation of GFP was performed at 900 nm by a femtosecond mode-locked (76 MHz repetition rate) Ti:Sapphire Mira900F laser pumped by a Verdi-V8 laser (both from Coherent, Santa Clara, CA). The laser beam was fed to the scanning head of a Leica TSC-SP2-AOBS confocal microscope. Fluorescence was collected on a multichannel plate photomultiplier (R3809U-50, Hamamatsu Photonics, Hamamatsu City, Japan) through a bandpass GFP filter at 515 ± 30 nm (EGFP-HQset by Analysentechnik, Lagenfeld, Germany). The fluorescence transients were acquired by using SPCIMAGE software (Becker & Hickl). The results were exported and analyzed by using an in-house-developed MATLAB (MathWorks, Natick, MA) toolbox. Images were acquired in 512×512 -pixel format, collecting in excess of 1,000 photons per pixel in 5–10 min, and about half this time when omitting the GFP emission filter. Photobleaching was between 5% and 10%. Acquisition speeds may be increased by reducing image size (≈ 1 min for 128×128 pixels) and by reducing the amount of oversampling or by the use of commercially available faster time-gated scanning FLIM systems (≈ 2 – 5 s per image at 128×128 or 265×265 pixels, respectively) or a wide-field frequency domain FLIM (≈ 0.1 – 0.5 s per image) to enable measurements of dynamic events (for a description and comparison of these systems, see ref. 21).

Ubiquitination was imaged in CHO cells expressing EGFP (pEGFP-C3 expression vector, Clontech) or GFP-PEST containing the mouse ornithine decarboxylase PEST sequence (pd2EGFP, Clontech) and REACH-ubiquitin constructs. Cells were cultured in DMEM containing 10% (vol/vol) FCS, $5 \mu\text{g}/\mu\text{l}$ penicillin-streptomycin, and 0.3 g/liter L-glutamine (Sigma-Aldrich). Cells were transfected by using the Effectene transfection reagent (Qiagen, Hilden, Germany), fixed with 4% (wt/vol) formaldehyde in PBS 18 h after transfection, and mounted in Mowiol (Aventis Pharma, Bad Soden, Germany).

Immunofluorescence and Western Blotting. Mouse monoclonal anti-HA Abs were from Covance Research Products (Columbia, MO; used at 1,000-fold dilution), Abs against ubiquitin were from Chemicon International (Hofheim, Germany; 1000-fold

dilution), Abs against GFP were from Roche Diagnostics (100-fold dilution), Cy5-conjugated secondary polyclonal goat-anti-mouse IgG F(ab')₂-fragments were from The Jackson Laboratory (300-fold dilution), and horseradish peroxidase-conjugated secondary polyclonal rabbit-anti-mouse Abs were from DAKO (3,000-fold dilution).

For immunofluorescence, CHO cells were fixed, washed three times in PBS, incubated 30 min in 0.01% Triton X-100 in PBS, blocked with 5% BSA in PBS for 1 h, incubated with primary Ab (anti-HA or anti-ubiquitin) for 2 h, and incubated with secondary Ab (Cy5-labeled goat-anti-mouse) for 1 h before mounting in Mowiol. Three 5-min washes in PBS were performed between each step.

For Western blotting, CHO cells expressing REACH-ubiquitin were cultured in a six-well tissue culture plate, scraped in boiling SDS/PAGE sample buffer, and subjected to gel electrophoresis. Samples were run on a reducing 12% acrylamide gel and blotted (Bio-Rad) onto a Protean BA83 nitrocellulose membrane (Schleicher & Schüll). The membrane was blocked with 5% nonfat skimmed milk for 1 h, incubated with primary Ab for 2 h, and incubated with secondary Ab for 1 h. Three 10-min washes were used between all steps. The membrane was then incubated with enhanced chemiluminescence (ECL) substrate (Amersham Pharmacia) and exposed to photographic film.

FqRET Analysis. Images of the GFP and Cy5 emission intensities were acquired by using the same Leica SP-2 microscope with single-photon excitation in confocal mode. The microscope is equipped with an acousto-optical beam splitter (AOBS), allowing custom emission wavelength selection. GFP was excited by using the 488-nm argon laser line; Cy5 was excited by using the 633 nm HeNe laser line. Fluorescence emission was collected in spectral windows of 495–530 and 640–750 nm for GFP and Cy5, respectively. Emission ratios were calculated, the resulting images were masked by using the fluorescence intensity of the GFP channel, and represented in a false-color lookup table by using custom-written MATLAB routines.

We thank Mr. A. Esposito for assistance and discussions, Mr. D. Lange for excellent technical support, and Dr. G. Bunt (Department of Cell Biology of Neuronal Signals, Max Planck Institute for Experimental Medicine, Göttingen, Germany) for the use of the spectrofluorimeter and discussions. This work was supported by a grant from the Deutsche Forschungsgemeinschaft (DFG) graduate program Neuronal Signaling and Cellular Biophysics GRK-723 (to S.G.) and by the DFG Center for Molecular Physiology of the Brain (to F.S.W.). The European Neuroscience Institute Göttingen is jointly funded by the Göttingen University Medical School, the Max Planck Society, and Schering AG.

1. Förster, T. (1948) *Ann. Phys.* **2**, 55–75.
2. Wouters, F. S., Verveer, P. J., & Bastiaens, P. I. (2001) *Trends Cell Biol.* **11**, 203–211.
3. Bunt, G. & Wouters, F. S. (2004) *Int. Rev. Cytol.* **237**, 205–277.
4. Siegel, R. M., Chan, F. K., Zacharias, D. A., Swofford, R., Holmes, K. L., Tsien, R. Y., & Lenardo, M. J. (2000) *Sci. STKE* **2000**, PL1.
5. Tsien, R. Y. (1998) *Annu. Rev. Biochem.* **67**, 509–544.
6. Rizzo, M. A., Springer, G. H., Granada, B., & Piston, D. W. (2004) *Nat. Biotechnol.* **22**, 445–449.
7. Karasawa, S., Araki, T., Nagai, T., Mizuno, H., & Miyawaki, A. (2004) *Biochem. J.* **381**, 307–312.
8. Clegg, R. M., Feddersen, B. A., Gratton, E., & Jovin, T. M. (1992) *Proc. SPIE Int. Soc. Opt. Eng.* **1640**, 448–460.
9. Squire, A. & Bastiaens, P. I. (1999) *J. Microsc.* **193**, 36–49.
10. Schönle, A., Glatz, M., & Hell, S. W. (2000) *Appl. Optics* **39**, 6306–6311.
11. Sytsma, J., Vroom, J. M., DeGrauw, C. J., & Gerritsen, H. C. (1998) *J. Microsc.* **191**, 39–51.
12. Becker, W., Bergmann, A., König, K., & Tirlapur, U. (2001) *Proc. SPIE Int. Soc. Opt. Eng.* **4262**, 414–419.
13. Matz, M. V., Fradkov, A. F., Labas, Y. A., Savitsky, A. P., Zaraisky, A. G., Markelov, M. L., & Lukyanov, S. A. (1999) *Nat. Biotechnol.* **17**, 969–973.
14. Shaner, N. C., Campbell, R. E., Steinbach, P. A., Giepmans, B. N., Palmer, A. E., & Tsien, R. Y. (2004) *Nat. Biotechnol.* **22**, 1567–1572.
15. Wang, L., Jackson, W. C., Steinbach, P. A., & Tsien, R. Y. (2004) *Proc. Natl. Acad. Sci. USA* **101**, 16745–16749.
16. Harpur, A. G., Wouters, F. S., & Bastiaens, P. I. (2001) *Nat. Biotechnol.* **19**, 167–169.
17. Neher, R. & Neher, E. (2004) *Microsc. Res. Tech.* **64**, 185–195.
18. Kummer, A. D., Kompa, C., Lossau, H., Pöllinger-Dammer, F., Michel-Beyerle, M. E., Silva, C. M., Bylina, E. J., Coleman, W. J., Yang, M. M., & Youvan, D. C. (1998) *Chem. Phys.* **237**, 183–193.
19. Patterson, G. H., Piston, D. W., & Barisas, B. G. (2000) *Anal. Biochem.* **284**, 438–440.
20. Li, X., Zhao, X., Fang, Y., Jiang, X., Duong, T., Fan, C., Huang, C. C., & Kain, S. R. (1998) *J. Biol. Chem.* **273**, 34970–34975.
21. Allen, P. G. (2003) *Nat. Cell Biol.* **5**, 972–979.
22. Harpur, A. G. & Bastiaens, P. I. H. (2001) in *Molecular Cloning: A Laboratory Manual*, eds Sambrook, J. & Russell, D. W. (Cold Spring Harbor Lab. Press, Woodbury, NY), Vol. 3, pp. 18.69–18.95.
23. Hänninen, P. E., Lehtelä, L., & Hell, S. W. (1996) *Optics Comm.* **130**, 29–33.
24. Fradkov, A. F., Verkhusha, V. V., Staroverov, D. B., Bulina, M. E., Yanushevich, Y. G., Martynov, V. I., Lukyanov, S., & Lukyanov, K. A. (2002) *Biochem. J.* **368**, 17–21.
25. Wiedenmann, J., Schenk, A., Rucker, C., Girod, A., Spindler, K. D., & Nienhaus, G. U. (2002) *Proc. Natl. Acad. Sci. USA* **99**, 11646–11651.
26. Yanushevich, Y. G., Staroverov, D. B., Savitsky, A. P., Fradkov, A. F., Gurskaya, N. G., Bulina, M. E., Lukyanov, K. A., & Lukyanov, S. A. (2002) *FEBS Lett.* **511**, 11–14.